MRS Advances © 2018 Materials Research Society
DOI: 10.1557/adv.2018.432

A New Subcritical Nanostructure of Graphene—Crinkle-Ruga Structure and Its Novel Properties

Ruizhi Li[1], Mrityunjay Kothari[1], Alexander K. Landauer[1], Moon-Hyun Cha[1], Heemin Kwon[1] and Kyung-Suk Kim[1]

[1]*Brown University, Providence, RI 02912, U.S.A.*

Abstract

Here, we report an experimental characterization of a new subcritical graphene nanostructure termed a crinkle ruga. Multilayer graphene forms crinkles as a periodic mode of buckling if the ratio of periodic buckling span to thickness is smaller than a critical value. Otherwise, it forms wrinkles. The crinkles have sawtooth-shaped profiles with their faces perfectly flat and the tips of the peaks and valleys highly curved. Our AFM measurements show that the width of the curvature focusing band at the tip is very narrow, e.g. smaller than 16 nm for a 6^o crinkle, indicating a strong influence of flexoelectric coupling in crinkle formation. We also found that concavity or convexity of crinkle tips, i.e. parity of the crinkle, can be controlled. Due to the flexoelectric coupling, the concave tip at the crinkle valley is positively charged, and the convex tip at the crinkle peak negatively charged. In addition, here, we demonstrate that the charges at the crinkle tips can attract macromolecules in adsorption experiments. We show linearly-aligned adsorption of C_{60} along crinkle valleys on an HOPG surface. In another experiment, we exhibit period-doubled adsorption of lambda DNA on an HOPG surface, possibly caused by ion kinetics involved in the DNA adsorption along the crinkle valleys.

INTRODUCTION

It has recently been found by Kothari *et al*. [1, 2] that freely suspended multilayer graphene (MLG) under lateral compression buckles to form periodic kink-shaped structures termed "crinkle ruga". Single layer graphene and few-layer graphene were previously known to exhibit characteristic dynamic ripples as well as static corrugations when suspended [3]. Traditionally, the buckling of a layered medium is known to bifurcate into a sinusoidal-shaped wrinkle morphology [4-6]. In contrast to wrinkles, crinkles have a sawtooth-shaped profile with highly localized curvature

distribution at the peaks and the valleys. Figures 1(a) and (b) demonstrate the geometric configurations of the crinkle versus the wrinkle modes of MLG buckling. Our density functional theory (DFT) study found that curvature is focused within boundary layers of width ~ 2 nm and the remaining span is essentially straight. The end angle θ_e for an elastic crinkle is very shallow (<6°). A critical number of atomic layers, N, is required to transition from the wrinkle-mode to the crinkle-mode for a given suspension length, $2L$. The $2L$-N phase diagram reproduced from [2] (see Figure 1(c) below) elucidates the theoretical requirements to construct an MLG crinkle. For MLG with tens to hundreds or more layers the criticality occurs when $2L \sim 13.9Na$ where a is the interlayer spacing, meaning that the crinkle configuration becomes energetically favorable at longer suspension lengths for thicker MLG.

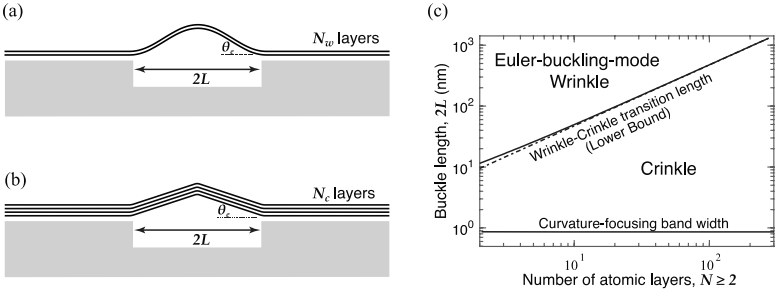

Figure 1. Schematics of (a) wrinkle-mode buckling of a slender MLG and (b) crinkle-mode buckling of low aspect ratio MLG hanging across a groove on an elastic substrate under compression; (c) Buckling phase map to show the domains of wrinkle and crinkle modes as governed by number of MLG layers (N) and MLG length ($2L$).

The criticality of MLG crinkling arises due to an electromechanical coupling of polarization and strain gradient, i.e. quantum flexoelectricity [7-9]. Kothari *et al.* [1] proposed an electromechanical model capturing the effects of flexoelectricity that predicts the formation of crinkles through a subcritical elastic bifurcation event. The combination of mechanical strain localization and flexoelectric amplification of curvature leads to the segregation of flexoelectric charges at crinkle peaks and valleys within a ~2 nm width. Both the flexoelectric line-type charges and crinkle angle depend directly on the end strain imposed on the suspended MLG.

In this paper, we develop an experimental program to generate peak-curvature-controllable (PCC) crinkles on the surface of a grooved substrate. The experiments demonstrate control of the crinkle parity, i.e. positive or negative curvature, and control of the magnitude of the peak curvature. The crinkle parity is controlled via details of groove geometries and substrate physical properties. The magnitude of the peak curvature is varied by both groove geometry and substrate strain. We also utilize natural crinkles on the surface of highly oriented pyrolytic graphite (HOPG) to demonstrate line charge concentration along the crinkle peaks and valleys by aligning Buckyballs (C_{60}) or DNA molecules on HOPG surfaces. Taken together, this suite of baseline experiments establishes PCC crinkles as a promising tool to manipulate a variety of charged and polarizable molecules at the nanoscale.

EXPERIMENTS

Peak Curvature Controllable Crinkles

To investigate quantum-flexoelectric crinkle formation, we laterally compress suspended MLG on two different grooved substrates: silicon (Figure 2(a-1)) and poly(methyl methacrylate) (PMMA) (Figure 2(b-1)). The MLG is prepared by mechanical exfoliation of HOPG (ZYH grade; Materials Quartz Inc., Strongville, OH) using the Scotch Tape technique [10]. With the mechanical exfoliation process we obtain MLG with thickness ranging between 40 nm and 70 nm, as confirmed by atomic force microscopy (AFM) height difference imaging in a later step. Freshly cleaved MLG is affixed onto the top surfaces of a pre-tensioned grooved substrate, such that the MLG is suspended over the grooves as in Figure 1(b). The pre-tension, applied by bending of the substrate to a controlled radius of curvature, was then released to compress the MLG layer. By accounting for the bending radius and crack-opening-type amplification behaviour the local, lateral end-point strain of the MLG is reliably controlled. To ensure a purely elastic crinkle, the maximum local compressive strain is designed to be 0.1% and 0.2% for the PMMA-MLG and the silicon-MLG assemblies respectively. We expect boundary layer slip mechanisms between the MLG and substrate surface to amplify the applied strain.

Substrate fabrication was conducted via two distinct processes. The grooved silicon was milled with a focused ion beam (FIB) using high-energy gallium ions (FEI-Helios). The final width (w) of grooves is ~500 nm, and the depth (h) is approximately 100 nm. A naturally occurring oxidation layer on the silicon surface promotes MLG adhesion. The PMMA grating patterns were prepared by reverse-molding a quartz diffraction grating with a rectangular groove pattern, and O_2 plasma surface treatment. The resulting geometry of grooves on the PMMA has width w = 1000 nm and height h = 500 nm and 50% groove fill-factor.

The final post-buckling configurations of MLG are imaged by AFM in either tapping (Asylum MFP-3D Origin) or non-contact mode (Park XE-Bio). The inset of Figure 2(a-2) shows an AFM image of the post-buckling configuration for the silicon-MLG specimen. The MLG buckles downward into the groove. As indicated by the theoretical predictions, the suspended MLG forms a shallow symmetrical kink with a kink angle $\theta_e \approx 6^\circ$, i.e. a crinkle, for the given applied strain. Figure 2(a-2) shows two ~100 nm AFM line scans from separate places along the axis of the crinkle (marked in the inset) around the crinkle valley. The profiles demonstrate that the crinkle has vanishingly little curvature on both sides, while the curved boundary layer is highly localized within the central ~16 nm span of the valley. The purely mechanical interlayer shear crinkling model of [2] for this configuration (500 nm free standing MLG with thickness ~ 60 nm and $\theta_e = 6°$) predicts the curvature boundary layer to be more than 25 nm. Given the presence of the AFM tip radius effect (AC160 probe, Asylum Research; R~10 nm), the localization region has reached the minimum detectable scale of AFM tip, which suggests that the real curvature boundary layer could be even smaller than 16 nm. The observed post-buckling configuration of suspended MLG indicates that the pronounced curvature localization of crinkles is beyond the level attributable to purely mechanical effects. Similarly, Figure 2(b-1) and (b-2) show the a schematic and a post-buckling AFM image of the PMMA-MLG specimen, respectively. The AFM image again shows the crinkle configuration. In this case, the crinkle buckles outward with a symmetrical kink angle of $\theta_e = 6°$.

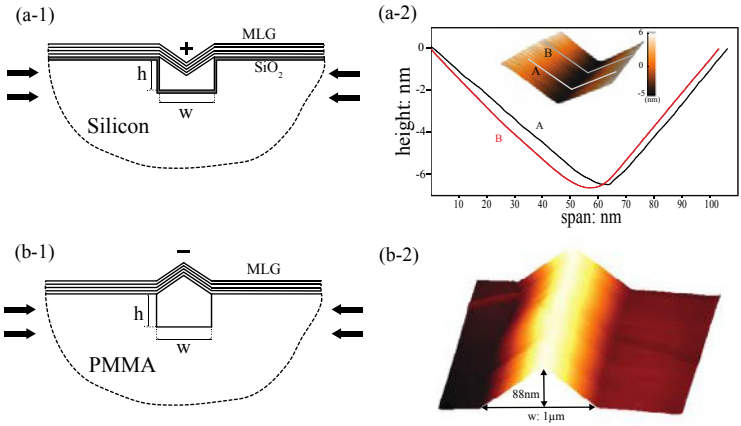

Figure 2. (a-1) A schematic of a P-type MLG crinkle on a silicon groove; (a-2) AFM image of the P-type MLG crinkle and two height profiles of the scans indicated on the AFM image. (b-1) A schematic of a N-type MLG crinkle on a PMMA groove; (a-2) AFM image of the N-type MLG crinkle: The height and the width of of the groove are depicted by h and w respectively.

Based on thorough AFM profilometry of our groove geometries and mechanical considerations we believe that the crinkle parity of suspended MLG depends on the substrate material and local contact geometry. Our analysis predicts that perfectly flat thin films suspended on perfectly rectangular grooves buckle outward for grooves under compression, as we observe in the PMMA-MLG specimen. In contrast, the grooves in our silicon substrate always show rounded corners due to the FIB machining process. The larger corner radius at the adhesion site provides an extended zone of van der Walls attraction between the silicon substrate surface and the MLG, which biases the MLG to buckle downward into the grooves. Further development of nanoscale buckling-parity control is required to fully reveal this behavior for a wider class of material pairs and groove geometries.

The highly localized curvature near a crinkle tip is a significant amplification of the peak curvature over a corresponding wrinkle mode: ~0.15 nm^{-1} with a 3^{o} kink for a 15 nm span or approximately 10-100 times more than the curvature of a wrinkle [2]. Due to the quantum flexoelectricity effect, this large strain gradient leads to high polarization density at crinkle. Consequently, upward versus downward buckling parities give different charge polarity along the crinkle lines. When crinkles buckle inward, as MLG on silicon gratings (Figure 2 (a-1) and (a-2)), positive effective charges accumulate along the crinkle valley, which we call 'P-type' crinkles. When crinkles buckle upward, as MLG on PMMA gratings (Figure 2 (b-1) and (b-2)), the negative charges concentration forms at crinkle ridge, which are 'N-type' crinkles.

Macromolecular Adsorption along HOPG Crinkles

The interaction potential depth between the crinkle line charges and charged or polarizable molecules is much deeper than the Boltzmann activation energy at room temperature [2], which implies that crinkles are preferred adsorption sites for polarized

molecules in solutions. We utilize this charge control effect of crinkles to adsorb Buckyballs (C_{60}) in linear arrays and lambda DNA on a freshly-cleaved HOPG surface to expose natural crinkles.

In the C_{60} adsorption experiment, 2 mg of C_{60} molecules (98%; Sigma-Aldrich) were suspended in 1 mL toluene (99.8%; Sigma-Aldrich). The solution was then sonicated for 30 minutes to accelerate C_{60} dissolution and achieve full saturation [11]. In the DNA experiment, refrigerated DNA-saline solution (500μg/mL; New England Biolab) was diluted with deionized water to the desired concentration (5μg/mL) [12]. Both solutions were kept at room temperature for 30 minutes and then pipetted onto a newly-cleaved HOPG surface. After molecular adsorption on the HOPG, and any remaining solution was carefully removed.

The HOPG surfaces after each adsorption experiment were then imaged via AFM. Figure 3 (a) is the topography of HOPG surface after C_{60} adsorption. This result shows the C_{60} molecules lining up to form one dimensional chains on the HOPG surface. The A-B line section (Figure 3(a) inset) shows that the height of C_{60} chain is ~ 0.6-0.8 nm, which is comparable to the scale of a single C_{60} molecule. The observed width of each C_{60} chain is over 10 nm, likely due to the radius effect of the AFM tip. We posit that the C_{60} chain-like patterns are due to the existence of HOPG crinkles. The line charges due to HOPG surface crinkles bias the adsorption of C_{60} molecules, which results in the ordered pattern of C_{60} chains.

DNA adsorption experiments reveal striking adsorption patterns as shown in Figure 3(b). While the DNA segments line up along straight lines individually, on a larger scale they form hexagonal patterns on the HOPG surface. The DNA molecules are confirmed by their height data in the A'-B' section line (Figure 3(b) inset). The small blobs at the top left of Figure 3(b) indicate salt recrystallization has also occurred. Comparing the A-B and A'-B' lines, the DNA spacing is almost half of that of the C_{60}. Also, in each hexagonal pattern, we often find more than one DNA molecule. The frequency doubling effect is discussed in the following section.

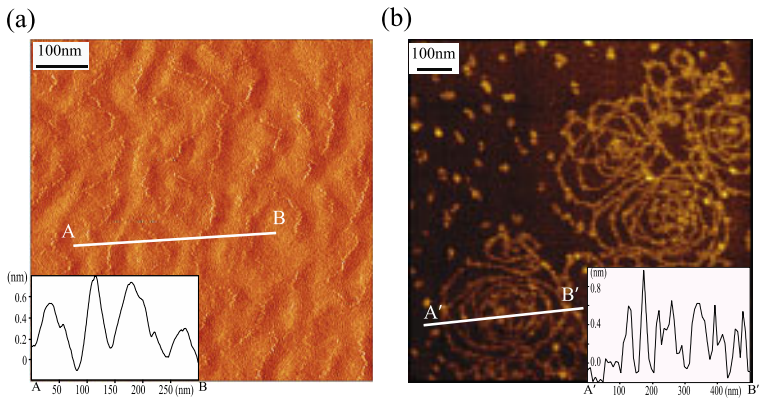

Figure 3. (a) AFM image of linear arrays of C_{60} adsorbed in a toluene solution on an HOPG surface. The height profile across the line A-B is displayed in the inset; (b) AFM image of adsorbed lambda DNA and precipitated salts of saline assay on an HOPG surface. The height profile across the line A'-B' is displayed in the inset; the interspacing of the adsorption lines is half of the crinkle spacing observed by the C_{60} adsorption experiment.

DISCUSSION

For the first time we present an experimental observation of the crinkle buckling shape. The fine scale AFM scan in the crinkle valley confirms the existence of a curvature localization boundary layer width as small as ~16 nm, which is less than the predicted pure mechanical crinkle boundary layer width, indicating flexoelectric coupling. Furthermore, the crinkles formation can be controlled. By adjusting the local compression, we can tune the end angle of crinkles and thus control the line charge density at crinkle peaks and valleys. The polarity of the crinkle line-charge can be altered by parity control during buckling of the suspended MLG. We obtain negative charge at the peaks of the upward N-type crinkle and positive charges in the P-type crinkle valleys. For this class of materials, the crinkle is in a purely elastic deformation domain, which indicates that charging and discharging of the crinkle line-charges can be fulfilled by simple loading and unloading the MLG.

The adsorption of macromolecules on the freshly-cleaved HOPG surface gives us insight into natural crinkles. Although we cannot detect these crinkles directly due to the limited measurement accuracy of the height, the adsorbed molecules illustrate patterns of crinkles on HOPG surface. Unlike one-dimensional artificial PCC crinkles, which are induced by uniaxial in-plane compression, the HOPG crinkles are generated through isotropic inhomogeneous residual stress in the HOPG structure. Therefore, the crinkle lines form two-dimensional patterns on the HOPG surface. For the C_{60} molecules, we observe C_{60} chains distributed randomly in multiple directions. Since the isotropic 2D crinkle patterns follows the symmetry of graphene atomic lattice, the long DNA chain is attracted by the crinkle pattern and spans multiple crinkles to form a hexagonal pattern on the HOPG surface.

A similar result for C_{60} adsorption is reported in [13] with scanning tunnelling microscopy (STM). The author attributed the C_{60} self-assembly along straight lines to nanoscale steps on the graphite surface. However, our AFM imaging shows all the C_{60} lines on a relative smooth graphite surface without changes in the graphene layer. Thus, we attribute the C_{60} organization to charging effects of crinkles on the same layer of graphite surface.

The hexagonal DNA patterns are also quite different from the DNA adsorption experiment on single or a few layers graphene [14], which does not show hexagonal or other organized arrangement in the adsorption patterns on the graphene surface. As we have indicated, the crinkles on HOPG surfaces are generated by a residual stress field in the HOPG structure. This stress field is caused by fabrication defects, such as sessile dislocations in the HOPG. With only one or a few layers of graphene, there is no residual stress field in the graphene structure, thus we cannot observe hexagonal or chain-like patterns of DNA on top of those surfaces. The existence of hexagonal DNA patterns only on HOPG surface again suggests it is the HOPG crinkles that cause adsorption patterns of DNA.

Comparing the interval between crinkle lines in C_{60} and DNA adsorption results, it is apparent that the DNA molecules have adsorption frequency doubling. Within one hexagonal shape of DNA molecules, there are two or more chains observed. The result is different from [15], where the DNA hexagon forms with less molecules. This is probably because transient ion kinetics involved in the adsorption process of the negatively charged lambda DNA on the positively charged crinkle valleys. The net linear charge density of the crinkle is only a fraction of the DNA and can partially neutralize the negative charge of the adsorbed DNA. Then, the interspacing between the adsorbed DNA molecules can create an adsorption potential valley for subsequent DNA adsorption.

CONCLUSIONS

In this research, a novel surface bifurcation buckling mode — the quantum-flexoelectric crinkle in MLG — is verified by compressing suspended MLG on grating substrates. Our experiments indicate that the crinkles are highly curvature-localized and their buckling direction parity can be altered by substrate properties and groove geometry. These crinkles are caused by mechanical and quantum flexoelectric effects and the concentrated line charges along crinkles attract charged or polarizable molecules. In the adsorption experiments, we observed 2D chain-like patterns on HOPG surface for both C_{60} and lambda DNA molecules. These patterns indicate the existence of crinkles on HOPG surface. The significant charge concentration as well as controllability of crinkles propose a future perspective to manipulate molecular alignment in the nanoscale.

ACKNOWLEDGMENTS

This work was supported by the U.S. National Science Foundation (Awards CMMI-1462785, 1563591, & DGE 1058262) for the experimental study by RL, AKL, HK & KSK, and the theoretical modeling by MK & KSK, and (Awards DMR-0520651 & XSEDE) for the DFT analysis by MHC & KSK. HK carried out the DNA adsorption experiment at Macrogen Inc. Korea, and the support from Macrogen is gratefully acknowledged.

References

[1] M. Kothari, M.-H. Cha and K.-S. Kim, Bull. Am. Phys. Soc. A30.00010 (2017).
[2] M. Kothari, M. H. Cha and K. S. Kim, Proc. Royal Soc. A. In publication (2018).
[3] A. Fasolino, J.H. Los and M.I. Katsnelson, Nat. Mater. **6** (11), 858-861 (2007).
[4] H.G. Allen, *Analysis and Design of Structural Sandwich Panels*, 1st ed. (Pergamon Press, Oxford, 1969).
[5] G. W. Hunt, L. S. Da Silva and G. M. E. Manzocchi, Proc. Royal Soc. Lond. A. **417** (1852), 155–177 (1988).
[6] J. H. Jung, J. Bae, M.-W. Moon, K.-S. Kim and J. Ihm, Solid State Commun. **222**, 14-17 (2015).
[7] T. Dumitrică, C. M. Landis and B. I. Yakobson, Chem. Phys. Lett. **360** (1-2), 182–188 (2002).
[8] S. V. Kalinin and V. Meunier, Phys. Rev. B. **77** (3), 033403 (2008).
[9] M. Zelisko, Y. Hanlumyuang, S. Yang, Y. Liu, C. Lei, J. Li, P. M. Ajayan and P. Sharma, Nat. Commun. **5**, 4284 (2014).
[10] K. S. Novoselov, A. K. Geim, S. V. Morozov, D. Jiang, Y. Zhang, S. V. Dubonos, I. V. Grigorieva and A. A. Firsov, Science. **306** (5696), 666-669 (2004).
[11] S. K. Klitgaard, K. Egeblad, L. T. Haahr, M. K. Hansen, D. Hansen J. Svagin and C. H. Christensen, Surf. Sci. **601** (9), L35-L38 (2007).
[12] Z. Liu, L. Zhao, Z. Zhou, T. Sun and Y. Zu, Scanning, **34** (5), 302-308 (2012).
[13] P. Dasmeh, J. Iran. Chem. Soc. **5** (2), 274-278 (2008).
[14] B. S. Husale, S. Sahoo, A. Radenovic, F. Traversi, P. Annibale and A. Kis, Langmuir. **26** (23), 18078-18082 (2010).
[15] Z. Liu, L. Zhao, Y. Zu, S. Tan, Y. Wang and Y. Zhang, Microsc. Microanal. **19** (3), 544-552 (2013).